THE JOURNAL OF Ammonia Energy

Available online at

jae.cardiffuniversitypress.org

ISSN **2752-7735**
The Journal of Ammonia Energy 01 (2023) 046–058

Cardiff University Press | Gwasg Prifysgol Caerdydd

Enhancement of the Catalytic Activity of Lithium Amide towards Ammonia Decomposition by Addition of Transition Metals

Brooker-Davis CA[a], Makepeace JW[a*], Wood TJ[b*]

[a]*School of Chemistry, Haworth Building, University of Birmingham, Birmingham, United Kingdom, B15 2TT*
[b]*ISIS Facility, Rutherford Appleton Laboratory, Harwell, Didcot, United Kingdom, OX11 0QX*

Abstract

The catalytic decomposition of ammonia to hydrogen is a vital process in the use of ammonia as a zero-carbon energy store. However, the viability of current catalyst systems in terms of operating conditions, versatility, and cost efficiency has proven an issue. Catalytic and gravimetric studies were conducted considering mechanistic uncertainty surrounding the enhanced catalytic activity reported for lithium amide and imide composited with transition metals (Cr, Mn, Fe). Gas flow in excess of ammonia decomposition was quantified and used to differentiate the extent of formation of non-stoichiometric lithium imide amide from other competing processes. This analysis showed the initial compositional transition from lithium amide to an imide-rich phase was reduced in temperature by compositing with Mn and Cr, but not with Fe. The system is therefore best considered as promoted lithium imide, with Cr and Mn acting to reduce the formation temperature of the active imide-rich phase such that the catalytic activity is enhanced.

© 2022 The Authors. Published by Cardiff University Press.
Selection and/or peer-review under responsibility of Cardiff University

Received: 10th Jan 23; Accepted: 9th May 23; Published: 4th July 23

Keywords: Ammonia decomposition, hydrogen production, lithium imide, lithium amide, catalytic promoter.

Introduction

To balance intermittency in the supply of renewable energy with fluctuations in demand, and to find a reasonable substitute for fossil fuels in transport, medium- to long-term energy storage solutions are required. Ammonia possesses a robust global infrastructure for production and distribution due to its critical role in the fertilizer industry. Its expanded implementation as a zero-carbon chemical energy store [1] is made possible by its relatively high energy density [2], comparative ease of liquefication [3,4], and low flammability [5]. However, the development of high-performing ammonia decomposition catalysts is crucial towards utilizing ammonia as an energy store, since its full or partial decomposition to hydrogen is prerequisite to use with many energy technologies [6]. For example, while ammonia may be used as a sustainable fuel by retrofitting current internal combustion engines [1], the partial cracking of supplied ammonia to release up to 4–5 wt% hydrogen is necessary to optimise its flammability range [7]. Additionally, proton exchange membrane fuel cells can be irreversibly damaged by < 1 ppm ammonia [8] and while solid oxide fuel cells are capable of tolerating direct ammonia [9], their high temperatures of operation have hindered commercialisation [1].

Ammonia decomposition catalysts have traditionally been formulated on supported transition metal nanoparticles, with ruthenium considered most active [10]; however, these systems often require very high operating temperatures to produce high-purity hydrogen. Metal-nitrogen-hydrogen (M-N-H) materials, including those based on sodium [11] and lithium [12], have emerged as comparable or superior catalysts to ruthenium systems and are comprised of relatively cheap, earth-abundant elements, making them more compatible with small scale power and transport applications. In particular, the lithium-nitrogen-hydrogen (Li-N-H) system shows ammonia conversion up to 1.5 times that of alumina-supported Ru by catalyst mass at moderate temperatures. This system is proposed to function by the formation of a solid solution between lithium amide ($LiNH_2$) and lithium imide (Li_2NH) (equation (1)) *via* the Frenkel defect-mediated release of NH_3, in which the bulk catalyst plays a significant role [13,14]. This imide-rich phase undergoes parallel decomposition and formation through a short-lived, lithium-rich intermediate to mediate the ammonia decomposition reaction (equation (2)). Lithium nitride hydride (Li_4NH) is a known decomposition product of lithium imide with an anti-Scheelite structure; it has also been shown to form anti-fluorite Li-N-H solid

* Corresponding authors. JWM: Tel.: +447500962522. E-mail address: J.W.Makepeace@bham.ac.uk TJW: Tel.: +447724191307. E-mail address: thomas.wood@stfc.ac.uk
https://doi.org/10.18573/jae.11 Published under CC BY-NC-ND license. This license allows reusers to copy and distribute the material in any medium or format in unadapted form only, for noncommercial purposes only, and only so long as attribution is given to the creator.

solutions [15–17], overall making it a likely catalytic intermediate *via* equations (3) and (4) [18].

$$(1+x)\mathrm{LiNH_2} \rightleftharpoons \mathrm{Li_{1+x}NH_{2-x}} + x\ \mathrm{NH_3} \quad (1)$$

$$\mathrm{NH_3} \rightleftharpoons \frac{1}{2}\mathrm{N_2} + \frac{3}{2}\mathrm{H_2} \quad (2)$$

$$2\mathrm{Li_2NH} \rightarrow \mathrm{Li_4NH} + \frac{1}{2}\mathrm{N_2} + \frac{1}{2}\mathrm{H_2} \quad (3)$$

$$\mathrm{Li_4NH} + \mathrm{NH_3} \rightarrow 2\mathrm{Li_2NH} + \mathrm{H_2} \quad (4)$$

There have been conflicting reports on the activity of lithium imide being further promoted through the addition of transition metals. Guo et al. demonstrated that the activity of lithium imide can be greatly enhanced by compositing with transition metals, proposing that an alternative catalytic mechanism *via* lithium ternary nitride intermediates (equations (5) and (6)) becomes accessible for these systems [19,20]. This would provide a lower energy pathway towards catalytic ammonia decomposition by effectively enacting the thermodynamic destabilisation of lithium imide.

$$\mathrm{Li_2NH} + \mathrm{TM} \rightarrow \mathrm{Li(TM)N} + \mathrm{H_2} \quad (5)$$

$$\mathrm{Li(TM)N} + \mathrm{NH_3} \rightarrow \mathrm{Li_2NH} + \mathrm{TM} + \mathrm{N_2} \quad (6)$$

In this study, it was reported that Li_2NH is inactive on its own and previous evidence on its performance was likely the product of a similar synergistic effect with the stainless steel reactor used [12,19], given the negligible activity seen for $LiNH_2$ in a copper-lined reactor [21]. However, *in situ* neutron diffraction studies showed that for lithium imide–manganese nitride and –iron nitride, $Li_xMn_{2-x}N$ was the only ternary phase which persisted in significant proportions at high ammonia conversions, while a Li_2NH-like phase persisted in both samples. This suggests bulk ternary nitride formation is not essential to the catalytic function of these systems [22], as further verified by isotopic studies [18]. Additionally, the lithium amide–ruthenium system is highly active in the absence of ternary nitride formation, highlighting the existence of an alternate mechanism of promotion [23]. A vacancy-enabled, dual-site mechanism of catalysis has been proposed in the cases of calcium imide–nickel for ammonia decomposition [24] and lanthanum nitride–nickel for ammonia synthesis [25]. In these systems, the presence of multiple active sites is suggested to facilitate the breaking of scaling relations which limit the overall productivity of traditional single-site catalysts, and it is possible Li-N-H–TM systems function *via* a similar pathway [26–29]. Given the ongoing uncertainty surrounding these systems, this report seeks to clarify the mechanism of activity enhancement in lithium amide–transition metal composite materials. This would enable a more targeted approach to catalyst design in the future and answer the question: in these systems, do transition metals function as catalysts, co-catalysts, or promoters?

Materials and Methods

Ammonia decomposition

$LiNH_2$ (0.5 g, Acros Organics, 95%), Mn (0.5 g, Sigma Aldrich, ≥99%, metallic impurities: 174.5 ppm Fe, 255.4 ppm Mg), Fe (0.5 g, Alfa Aesar, 98%, no trace element analysis) and Cr (0.5 g, Alfa Aesar, 99%, metallic impurities: 740 ppm Fe) were used as supplied. Composite catalysts were prepared by hand grinding $LiNH_2$ (0.5 g) with Cr, Mn, or Fe (0.5 g) for five minutes in an argon-filled glove box; no bulk reaction is expected through mechanical grinding alone [22]. Catalyst materials were sealed inside a cylindrical 21 cm^3 stainless steel 316L reactor (Cambridge Reactor Design) configured for gas flow over the catalyst, before being transferred anaerobically to a vertical tube furnace and attached to a gas flow panel (Fig. 1).

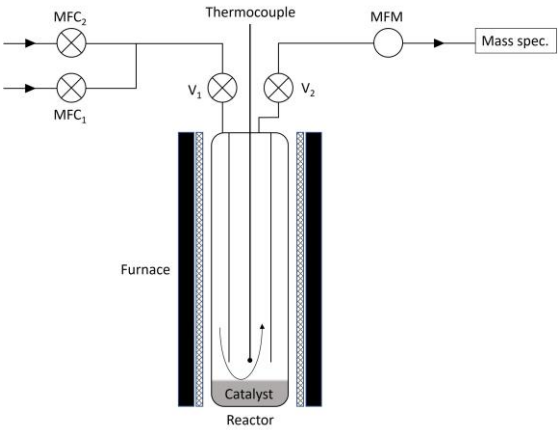

Fig. 1. Schematic illustration of the gas flow panel, where V_1 and V_2 are the inlet and outlet valves, MFC_1 and MFC_2 are mass flow controllers, and MFM is the mass flow meter. The arrow represents the 'flow over' tube-in-tube geometry of the reactor.

The flow of argon and ammonia into the system was regulated by mass flow controllers (HFC-302, Teledyne Hastings Instruments) and outlet gas flow was measured by a mass flow meter (HFM-300, Teledyne Hastings Instruments). Analysis of the exhaust gas composition was carried out using a mass spectrometer (MS) (Hidden Analytical HPR-20 QIC R&D, m/z = 1–40). The panel was evacuated up to the reactor before being flushed with ammonia to reduce air contamination prior to the start of the experiment.

The ammonia conversion efficiency of catalyst materials was measured similarly to previous reports [11,12,30]. Experiments were carried out under a 30 sccm flow of ammonia (99.98%, refrigerant grade,

BOC) at atmospheric pressure, following a 28-hour in-house program (OpenGenie, written using LabView) in which temperature was raised incrementally from 300 to 540°C. The MS was calibrated using known gas mixtures to establish the fragmentation ratio (or distribution of m/z values and intensities) and ionization factor (or ionization efficiency relative to argon) for each gas species. A second calibration to ammonia was carried out to mitigate drift in the hydrogen ionization factor. Consequently, the ammonia gas fraction could be inferred throughout each experiment and, by averaging this over each 2–3 h temperature dwell, the ammonia conversion efficiency of the catalyst at various temperatures was determined. These data were fitted using the Levenberg-Marquardt algorithm to a Gompertz curve, reflecting the kinetic behaviour of the systems. Results are reported relative to the blank reactor, which possesses limited activity towards ammonia decomposition.

Gas flow analysis

The flow of each component gas was quantified by combining mass flow and MS data using bespoke Python code. Briefly, any additional volume of gas released was quantified by integrating the gas flow following subtraction of the gas flow attributed to ongoing ammonia decomposition. The stoichiometry of the $LiNH_2$–Li_2NH solid solution could then be calculated at each temperature.

Gravimetric analysis

Simultaneous thermal analysis (Netzsch STA 449 F1 Jupiter) was used to study the decomposition of lithium amide under an inert N_2 atmosphere using combined techniques of thermogravimetry (TG), differential thermal analysis (DTA), and MS. 24.3 mg of $LiNH_2$ (95%, hydrogen storage grade, Sigma Aldrich) or 48.6 mg of its 1:1 mass composite with Cr (99%, Thermo Fisher Scientific), Mn (99.95%, Alfa Aesar), or Fe (99.99%, Sigma Aldrich), was loaded into an alumina crucible and enclosed with an apertured alumina lid inside an argon-filled glove box. Samples were transferred to the instrument and heated by 5°C min^{-1} to 550°C under a 70 sccm flow of nitrogen.

X-ray powder diffraction

X-ray powder diffraction (XRD) measurements were conducted on post-catalytic materials employing either a PANalytical X'Pert Alpha diffractometer using copper Kα_1 radiation or a STOE STADI P diffractometer using molybdenum Kα_1 radiation. A small number of samples were also studied using high-resolution XRD at the I11 beamline, Diamond Light Source (λ = 0.8268226 Å). Rietveld analysis was carried out for each diffraction pattern using the TOPAS Academic v7 package.

Results

Ammonia decomposition experiments

The gas flow data for the blank reactor ammonia decomposition experiment and the experimental temperature program are shown in Fig. 2 a) and b). These will be discussed here as the baseline case, from which differences in the data for the catalyst samples can be interpreted. The flow data follow a similar profile to the temperature program, reflecting the increased conversion of ammonia to nitrogen and hydrogen at higher temperature, with equilibrium conversion values obtained during each temperature dwell.

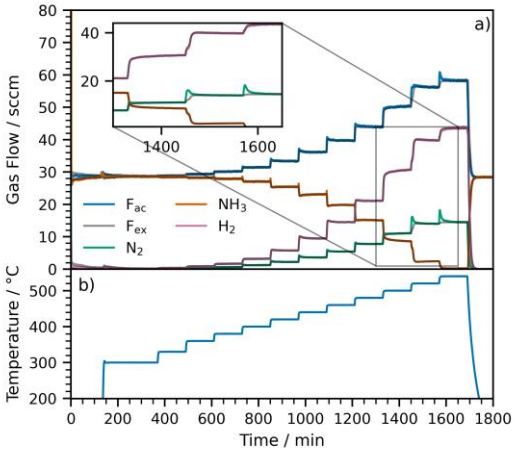

Fig. 2. a) Component (NH_3, N_2, H_2) and total (F_{ac}) gas flows and the flow expected if only ammonia decomposition were occurring (F_{ex}) for the blank reactor ammonia decomposition experiment, and b) details of the experimental temperature program. An initial 120 min dwell at room temperature is not used in later experiments.

The total gas flow approximately doubles from 30 to 60 sccm during the experiment, which is expected from the stoichiometry of the ammonia decomposition reaction. Additionally, there are several examples where the flows deviate from those expected due to ammonia decomposition alone (F_{ex}): during the temperature rise to 300°C (140 min), a small release of H_2 and simultaneous absorption of NH_3 occur, and two large releases of N_2 are seen from 1440–1560 min (Fig. 2 a) inset). These correspond with reactor nitriding and denitriding processes respectively, equations (7) and (8).

$$x\mathrm{Fe} + \mathrm{NH_3} \rightleftharpoons \mathrm{Fe}_x\mathrm{N} + \frac{3}{2}\mathrm{H_2} \quad (7)$$

$$\mathrm{Fe}_x\mathrm{N} \rightarrow x\mathrm{Fe} + \frac{1}{2}\mathrm{N_2} \quad (8)$$

Iron denitriding is largely dependent on the partial pressure of hydrogen [31], hence major N_2 release is not observed until temperatures at which considerable ammonia conversion occurs. After the

temperature rise to 520°C, the increase in ammonia conversion is partially attributed to Fe being more catalytically active than Fe_xN [32]. These features are present in all other experiments.

Ammonia decomposition experiments were conducted on $LiNH_2$, Cr, Mn, and Fe as single-component catalysts and within $LiNH_2$–TM composites (Fig. 3). Gas flow data of the transition metal-only experiments (Figs. S1–3, ESI) largely resembled results for the blank reactor, illustrating the limited activity of these metals towards catalysing ammonia decomposition.

[34] but $LiNH_2$ can accommodate only a small amount of non-stoichiometry. The $LiNH_2$-only release and absorption were each fitted to an exponential time constant of 1.15(4) min (Fig. S4), verifying their relation to the same reaction process.

The significant release of all gases at 960 min (temperature rise to 460°C) shown enlarged (Fig. 3 a)) is assigned to a compositional change from molten $LiNH_2$ to the imide-dominant, $Fm\bar{3}m$ solid solution phase, $Li_{1+x}NH_{2-x}$ ($0 \leq x \leq 1$, equation (1)), consistent with *in situ* neutron diffraction studies of this non-stoichiometric phase evolution under

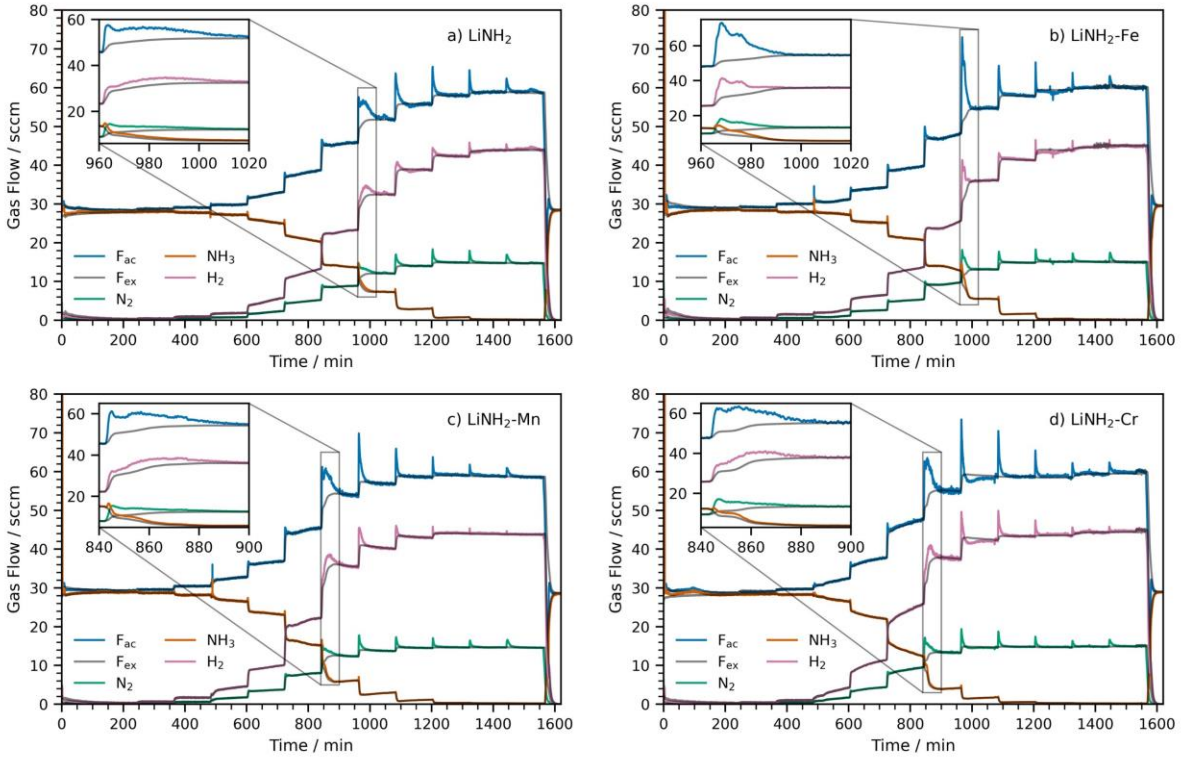

Fig. 3. Total, component, and expected gas flows for the a) $LiNH_2$ (0.5 g), b) $LiNH_2$–Fe, c) $LiNH_2$–Mn, and d) $LiNH_2$–Cr (1 g) ammonia decomposition experiments.

For $LiNH_2$-containing experiments, the catalyst composition is expected to change upon conversion of $LiNH_2$ to Li_2NH *via* solid solution phases as the temperature rises. This manifests in additional gas flow increases exceeding the expected flow variation, as according to equations (1–4). For all four experiments, a fluctuation in the ammonia flow is seen during the temperature rise to 380°C (480 min). The initial absorption and then release of ammonia is consistent with the melt of lithium amide, which has a reported melting point of 375°C [33]. Ammonia uptake is thought to arise from imide impurities in stock $LiNH_2$ before the onset of limited lithium amide decomposition via the reverse process (equation (1)), since the diffusion of NH_2^- and H^+ species is less kinetically hindered in the molten salt

ammonia decomposition conditions [12]. As described previously, the background-subtracted component gas flows were integrated and volumes of NH_3 and H_2 releases used to calculate the $Li_{1+x}NH_{2-x}$ stoichiometry following flow re-equilibration. At this temperature, the $Li_{1+x}NH_{2-x}$ stoichiometry reaches a limiting value, suggested to be around x = 0.333 [17], at which point a thermodynamically-driven transformation to the solid solution phase occurs. This results in the release of ammonia (and nitrogen and hydrogen by its subsequent decomposition) and significant increase in the value of *x*. The long decay of these gas releases may correspond with a non-stoichiometric continuum being formed, where the catalytic activity increases with *x* (nearing full

lithium imide stoichiometry). Further gas releases are associated with the value of x continuing to increase with temperature and reactor denitriding, which begins at lower temperatures than for the blank reactor since the partial pressure of hydrogen increases faster when catalyst is present. The absorption of all gases during cool down under ammonia reflects the re-formation of lithium amide (equation (1)) and highlights the reversibility of this reaction (Fig. S5, ESI).

Interestingly, while the component gas flows measured during the $LiNH_2$–Fe experiment (Fig. 3 b)) closely resemble those of the $LiNH_2$ experiment, the large flow deviation during $LiNH_2$–Mn (Figure 3 c)) and $LiNH_2$–Cr (Figure 3 d)) studies appears during the lower temperature rise to 440°C (840 min). This is consistent with the phase transition from molten lithium amide to the $Fm\bar{3}m$ phase occurring at a lower temperature for –Cr and –Mn composite systems compared with $LiNH_2$ and $LiNH_2$–Fe.

Evidence for the formation of lithium nitride hydride

Following the formation of lithium imide amide, the catalytic cycle of ammonia decomposition is assumed to proceed through a lithium-rich intermediate. However, previous, indirect evidence has been inconclusive regarding the identification of this intermediate as lithium nitride hydride [17,35] or a lithium ternary nitride [19–21]. Examining the background-subtracted, component gas flow data at 1320 min (Fig. 4 a)), which occurs after the major transition to the imide-rich solid solution phase but before reactor denitriding begins to play a dominant role in the system's non-equilibrium behaviour (Fig. 4 c)), it appears that N_2 and H_2 release profiles are initially very similar and peak at comparable values, around 3.1 and 3.4 sccm, respectively. The flow of hydrogen subsequently drops to less than expected from ammonia decomposition; this is indicative of H_2 absorption, and is simultaneous to a slowly decaying N_2 signal.

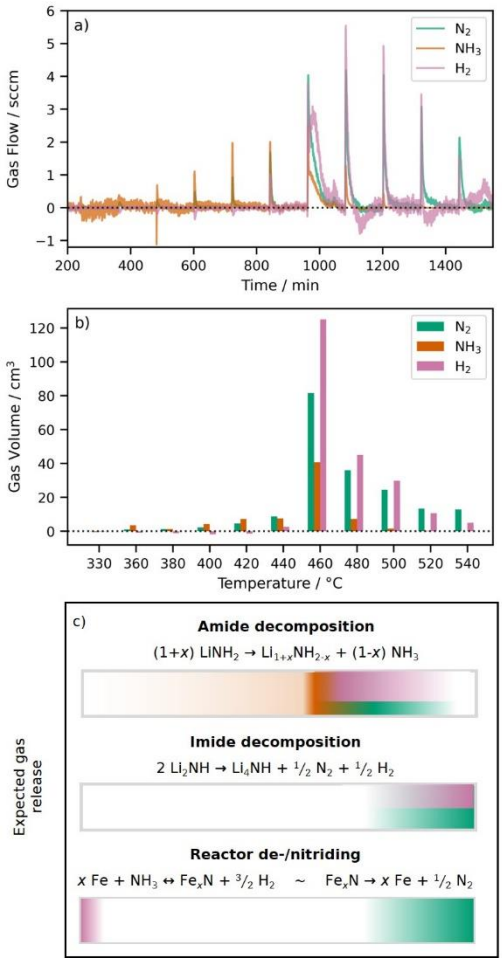

Fig. 4. For the $LiNH_2$ experiment, a) component gas flow data with ammonia decomposition background subtracted, where the black dotted line represents the flow expected from only ammonia decomposition occurring, b) component gas release volumes calculated by integrating the gas flow data during each temperature rise, and c) component gas release expected from each competing reaction process as temperature increases.

These observations are suggestive of multiple, overlapping, non-equilibrium processes, where the absorption of hydrogen is taken to imply that the slower process is the denitriding of the reactor, and the faster process is some combination of the $Li_{1+x}NH_{2-x}$ stoichiometry changing and lithium nitride hydride formation. Given the approximately 1:1 N_2:H_2 molar ratio and negligible NH_3 release shown in the integrated gas release volume data (compared with the temperature rise to 460°C, Fig. 4 b)), these gas releases may be further indirect evidence of Li_4NH formation.

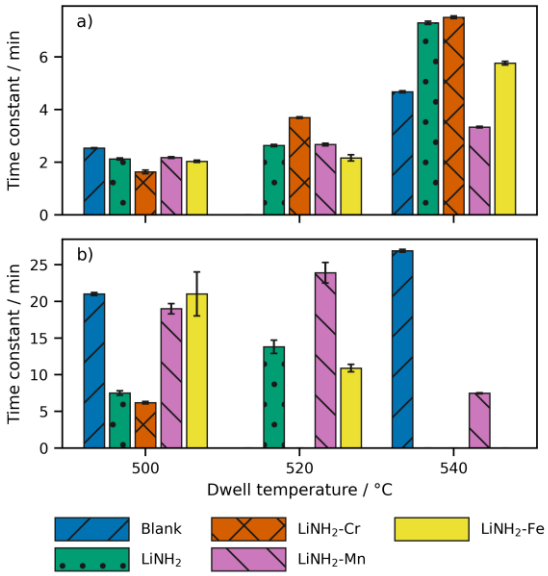

Fig. 5. Time constants obtained from exponential fits to the nitrogen release data during the final three temperature increases of blank reactor, $LiNH_2$, $LiNH_2$-Cr, $LiNH_2$-Mn, and $LiNH_2$-Fe experiments. Where the nitrogen release has been fit to two exponential curves, two-time constants are given. A reasonable fit to the 520°C nitrogen release could not be obtained for the blank reactor.

Similar results are obtained during each of the temperature increments from 480–540°C, although reactor denitriding becomes increasingly dominant as the temperature is increased [31]. The formation of Li_4NH following the phase transition at 460°C can been physically reasoned as a consequence of N^{3-} and H^- groups being stabilised by migration into the bulk of the material, which in this way acts as a thermodynamic sink for reactive species [17,36].

For each system, the nitrogen gas release data associated with each of the final three temperatures were fitted with one or two exponential curves (Fig. S6–S19, ESI) and the time constants for each process are given in Fig. 5 (Raw data can be found in Table S1, ESI). As discussed previously, the slow process in each case is interpreted as denitriding of the reactor, leaving the faster process to be understood in terms of the behaviour of the catalyst system. For each system, this time constant increases with temperature. This is consistent with lithium nitride hydride formation, since the occupancy of highly charged N^{3-} anions within the solid solution phase would likely inhibit the migration of NH^{2-} anions [17] and thus prevent N_2 and H_2 formation and release, increasingly disfavouring the further decomposition of lithium imide.

Correlations between catalytic activity and non-stoichiometry in $Li_{1+x}NH_{2-x}$

The ammonia conversion efficiency of each system is plotted in Fig. 6 a) and compared with the average stoichiometry in the lithium imide amide solid solution.

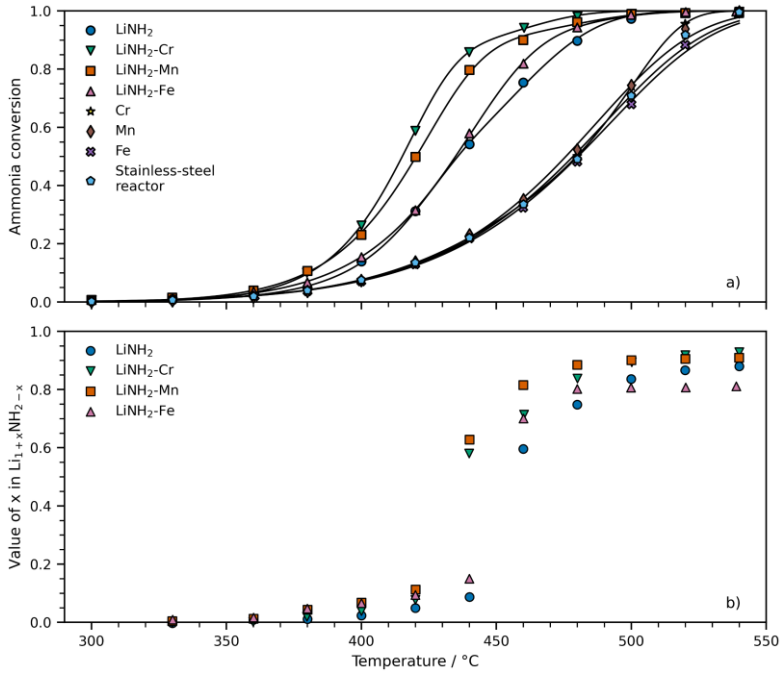

Fig. 6. a) Variable temperature ammonia conversion efficiency of $LiNH_2$, Cr, Mn, Fe, blank, and $LiNH_2$-composite materials, with sigmoidal fits to the data (black lines), and b) temperature dependent value of x in the imide amide solid solution for $LiNH_2$ and composite systems.

System	Value of x in $Li_{1+x}NH_{2-x}$	Ammonia conversion	H_2 production rate per mass of catalyst / $mmol_{H_2} g_{cat}^{-1} h^{-1}$	H_2 production rate per mass of $LiNH_2$ / $mmol_{H_2} g_{LiNH2}^{-1} h^{-1}$
$LiNH_2$	0.09	0.54	0.80	0.80
$LiNH_2$-Cr	0.58	0.86	0.65	1.30
$LiNH_2$-Mn	0.63	0.80	0.62	1.24
$LiNH_2$-Fe	0.15	0.58	0.42	0.84

Table 1. Extent of ammonia conversion, value of x in the lithium imide amide solid solution, and H_2 production rate per overall mass of catalyst and per mass of $LiNH_2$ (active component) for $LiNH_2$, $LiNH_2$-Cr, $LiNH_2$-Mn, and $LiNH_2$-Fe at 440°C.

From the stoichiometry calculation, it is confirmed that the large gas release relates to the phase transition from $LiNH_2$ to $Li_{1+x}NH_{2-x}$ as discussed, which appears as a significant increase in the value of x at 440°C ($LiNH_2$–Cr and $LiNH_2$–Mn) or 460°C ($LiNH_2$ and $LiNH_2$–Fe). This is related to a steep acceleration in the conversion of ammonia for all systems with both datasets possessing a similar, sigmoidal profile, and implies that lithium amide itself is inactive towards ammonia decomposition, with catalytic activity effectively being 'switched on' by the formation of $Li_{1+x}NH_{2-x}$ [12,36]. Importantly, the lower temperature phase transition for $LiNH_2$-Cr and $LiNH_2$-Mn systems is correlated with an enhanced ammonia conversion for these two systems. This is highlighted in Table 1 that shows for $LiNH_2$–Cr and –Mn systems which possess greater imide character (higher x) at 440°C, the ammonia conversion is around 1.5 times greater than that of $LiNH_2$. The elevated activity is emphasised also in the hydrogen production rate per gram of $LiNH_2$, confirming that if $LiNH_2$ is considered as the active catalytic component, its activity is promoted by compositing with Cr or Mn.

The hydrogen production rate per mass of catalyst is a valuable measure of the mass efficiency of each system however it fails to capture inter-system trends which result from the effect of transition metals compared with $LiNH_2$ on its own. Since the transition metals on their own perform very similarly to the blank reactor, activity enhancement cannot be explained by a linear combination of the activity of the two independent components. Instead, the effect is necessarily a result of some interaction between the transition metals, Cr and Mn, and $LiNH_2$, which does not exist for Fe. Given the already high activity of the $LiNH_2$-only system and observed reduction in the formation temperature of $Li_{1+x}NH_{2-x}$ in the enhanced systems, this ameliorative effect is proposed to involve the transition metal-mediated destabilisation of $LiNH_2$, such that the active, imide-like phase is present at lower temperatures. This could resemble the well understood thermodynamic destabilization of $LiNH_2$ and similar compounds, often investigated with the intention of reducing the material's decomposition temperature and thereby optimising its hydrogen storage properties [37–41]. For the composite systems reported here, this may involve the formation of thermodynamically favourable ternary phases and/or an electronic interaction which weakens Li-N/N-H bonds. The active phase is consequently able to catalyse ammonia decomposition through the Li_4NH intermediate beginning at lower temperatures, *via* a TM-promoted reaction scheme as summarised in Fig. 7.

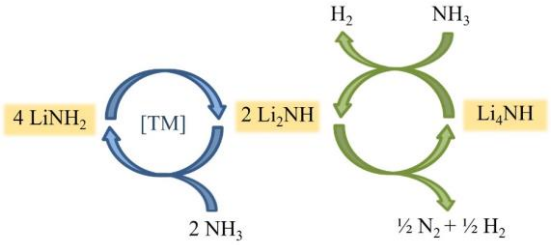

Fig. 7. Proposed reaction scheme of Li-N-H–TM composite materials for ammonia decomposition.

Thermogravimetric analysis

Gravimetric studies of $LiNH_2$ and its composites with Cr, Mn, and Fe were conducted to examine the amide decomposition reaction under an inert nitrogen atmosphere; data obtained are shown in Fig. 8, where ammonia conversion data are reproduced for comparison in panel a) (raw STA data can be found in the ESI, Figure S20).

The overall decomposition of $LiNH_2$ to the Li_2NH-dominant, $Fm\bar{3}m$ solid solution by equation (1) [12] is evidenced by a loss in sample mass and coincident increase in the m/z=17 MS signal, as observed in each experiment. The onset of this mass loss follows immediately after the melt of lithium amide, which was interpreted from a large endotherm at around 368°C for the $LiNH_2$ experiment (Fig. 9 c)). A minor endotherm at 525°C observed during this experiment could relate to small amounts of Li_4NH forming in the solid solution [17], with this decomposition pathway having been previously reported at 550°C under an inert atmosphere [15], although only a very small increase in the m/z=2 H_2 signal is seen at this point.

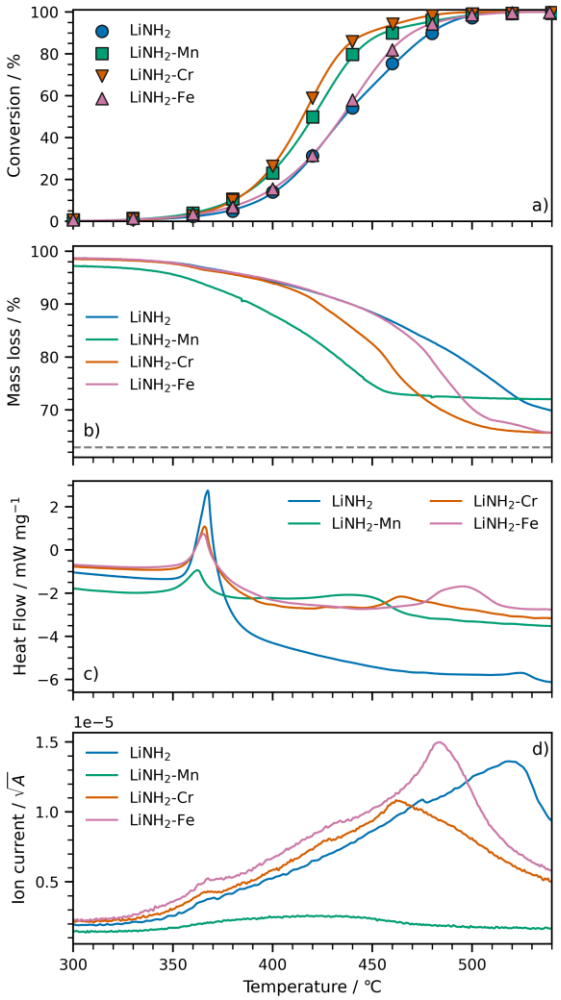

Fig. 8. For each $LiNH_2$(–TM) system, a) ammonia conversion data, b) gravimetric data relative to the starting mass of $LiNH_2$, where the dashed line indicates the mass loss expected from complete $LiNH_2$ decomposition (37.1%), c) differential thermal analysis, and d) ammonia (m/z=17) MS trace of STA exhaust gases.

The mass loss was less than expected from complete $LiNH_2$ decomposition in each case, partially owing to the fast ramp rate used during these measurements, but also to the formation of lithium ternary nitrides [22,42]. This latter process is evidenced by the high temperature (> 400°C) endotherms and H_2 release in composite experiments (Fig. 8 c), Fig. S20, ESI). Ternary nitrides likely accounted for only a very small amount of the sample in the case of $LiNH_2$–Fe, as predicted thermodynamically (Figure S22 a), ESI), since mass loss closely approached the expected from $LiNH_2$ decomposition and exceeded that expected for Li_3FeN_2 formation (29.1%). Similarly, for $LiNH_2$–Cr, no ternary nitrides were visible in the XRD pattern of the post-reaction sample from a replicated experiment under argon flow (Fig. S21, ESI). Although there exist thermodynamically accessible ternary nitrides in this system (Fig. S22 c), ESI), it is likely these are only present in low concentrations and/or there is a kinetic barrier to their formation. By contrast, there are a number of ternary nitrides thermodynamically accessible from the $LiNH_2$–Mn system (Fig.S22 b), ESI) and correspondingly the significant formation of both binary and ternary nitrides (97.9(11)% by mass of the post-reaction sample, Fig. S23, ESI), resulted in a plateau at a much lower mass loss than expected from $LiNH_2$ formation. Since this raises the question of the role of N_2 in the metal nitriding reactions and its possible confounding influence on the thermogravimetric behaviour of the system, a second $LiNH_2$–Mn experiment was performed, this time using Ar as the purge gas (Fig. S24, ESI). Results showed that very little change in the TG profile is observed in the absence of an external source of nitrogen, indicating that the metal nitriding reactions are largely initiated by lithium imide amide as an active source of nitrogen, and thus $N_{2\,(g)}$ is inert under these conditions. Hence, a conclusive mass-activity relationship is demonstrated across the series of samples, in which the ammonia conversion and mass each begin changing at around 350°C following the onset of $LiNH_2$ decomposition. This offers further evidence towards the inactivity of $LiNH_2$ alone and the implication of $Li_{1+x}NH_{2-x}$ as the primary catalytic component. Additionally, inter-system trends are similar between the catalytic and thermogravimetric datasets, with $LiNH_2$ and $LiNH_2$–Fe possessing mass loss profiles which are near identical until 450°C, while $LiNH_2$–Cr and $LiNH_2$–Mn systems begin losing mass at a lower temperature than $LiNH_2$.

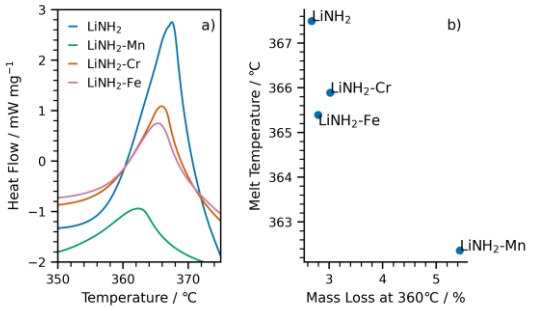

Fig. 9. Differential thermal analysis data around the melting point of $LiNH_2$, and b) correlation between the $LiNH_2$ melt temperature as identified from the DTA maxima and the mass loss at 360°C, just prior to the melting point.

These trends are reproduced in the m/z=17 MS data, which are expected to be representative of the $LiNH_2$ decomposition reaction because ternary nitride formation contributes little to the NH_3 release (NH_3 release is not well correlated with H_2 or DTA traces, Fig. 8 c), Fig. S20, ESI). These results overall provide further evidence towards the formation of $Li_{1+x}NH_{2-x}$ being the catalytically important step.

The melt endotherm of lithium amide (Fig. 9 a)) additionally shows inter-system variation, with maxima indicating that the melting point of $LiNH_2$ differs between samples in the order: $LiNH_2$ > $LiNH_2$–Cr ≈ $LiNH_2$–Fe > $LiNH_2$–Mn. This is consistent with varying extents of imide incorporation into the $I\bar{4}$ tetragonal lattice of $LiNH_2$ at temperatures below the melting point (i.e., pre-melt decomposition of the amide), which introduces structural disorder and thus reduce its fusion enthalpy [43]. The trend in this process is emphasised in Fig. 9 b), which shows for systems with greater mass loss below the melting temperature, the melt temperature is lower.

Post-reaction structural characterisation

Characterisation of the post-catalytic samples was undertaken using X-ray powder diffraction. XRD patterns for the $LiNH_2$, $LiNH_2$–Cr, $LiNH_2$–Mn, and $LiNH_2$–Fe samples are shown in Fig. 10; transition metal post-catalytic samples consisted of only the

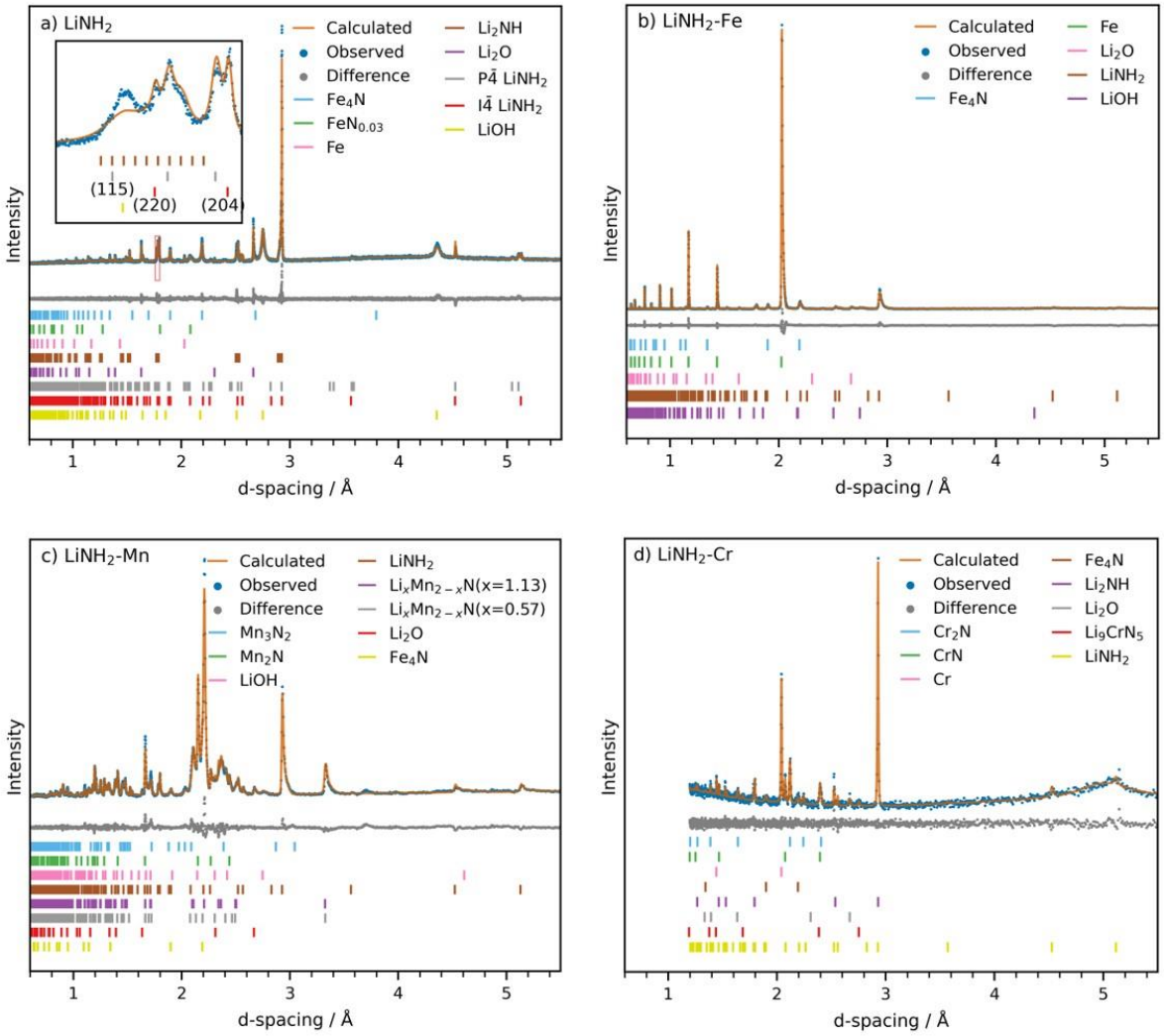

Fig. 10. X-ray powder diffraction data collected from the post-catalytic materials of a) $LiNH_2$, b) $LiNH_2$–Fe, c) $LiNH_2$–Mn, and d) $LiNH_2$-–Cr ammonia decomposition experiments. Plotted are the observed data (blue), the fit calculated by Rietveld analysis (orange), the difference between them (grey), and tick marks showing the expected positions of Bragg peaks for each of the included phases. The inset in a) shows an example complex peak attributed to the imide amide non-stoichiometry, which results from the overlapping (115) and (204) $LiNH_2$, and (220) $LiNH_2$ and $Li_{1+x}NH_{2-x}$ (and (200) LiOH impurity) Bragg reflections.

various transition metals and their binary nitrides (Figs. S25–S27, ESI).

For the $LiNH_2$ recovered material, best fit to the high-resolution data was obtained by refining ten, evenly spaced $Li_{1+x}NH_{2-x}$ stoichiometries, where the *a* lattice parameter decreases linearly as *x* increases [13]. In addition to the end member species, $I\bar{4}$ and $P\bar{4}$ $LiNH_2$ and $Fm\bar{3}m$ Li_2NH, the non-stoichiometry in the post-catalytic Li-N-H material is exemplified by the complex peak shown enlarged (Fig. 10 a)) inset), where the broad feature results from the continuum in lithium imide amide stoichiometry. The average lithium imide stoichiometry was refined to $Li_{1.18}NH_{1.82}$; this is consistent with the value of *x* calculated after cooling under ammonia from the gas release data ($Li_{1.30}NH_{1.70}$), given the sample remained under ammonia for longer before the XRD measurement was taken. This highlights the reversibility of equation (1) *via* NH_3 absorption of lithium imide to re-form lithium amide during the cool down stage.

While only the re-formed starting materials and impurity phases were present in the post-catalytic material from the $LiNH_2$–Fe experiment, $LiNH_2$–Cr and $LiNH_2$–Mn samples showed a greater complexity in their XRD patterns. A ternary nitride, Li_9CrN_5 and $Li_xMn_{2-x}N$ respectively, was present in each case, the former of which was previously observed in similar studies by Guo et al. [19] and the latter during *in situ* studies under ammonia decomposition conditions [22]. Two lithium occupancies in the Pnnm $Li_xMn_{2-x}N$ phase ($x = 0.57$ and $x = 1.13$) were refined to obtain best fit to the $LiNH_2$–Mn data. This is appropriate since prior characterisation of this phase showed that it can accommodate variable stoichiometry, and similar trends to prior reports were demonstrated in the orthorhombic distortion growing more significant with increasing lithium occupancy [44]. Additionally, hexagonal ($P6_3/mmc$) Cr_2N and Mn_2N phases were present, which ordinarily are not formed under these conditions in the corresponding TM-N system [45,46]. This suggests these may be $Li_xM_{2-x}N$ phases, with small amounts of Li occupancy stabilising them at lower temperatures. Given these measurements were carried out *ex situ* after cooling under ammonia, it is unclear how the post-catalytic composition reflects the active catalyst at high ammonia conversions, although *in situ* studies revealed $Li_xMn_{2-x}N$ in the catalytic regime for the Li_2NH–MnN system [22]. While the role of these ternary nitride phases remains unclear, given the catalytic and gravimetric evidence for the major role of lithium imide amide in the catalytic reaction, it is unlikely these are essential to the catalytic effect. Additionally, samples retrieved post-catalysis were predominantly the reformed starting materials or phases which decompose to the active solid solution under ammonia decomposition conditions [22,44]. Previous studies have evidenced the longer term (≤ 25 h) durability of similar Li-N-H–TM catalysts undergoing ammonia cracking, for example MnN–Li_2NH was shown to demonstrate negligible activity loss over 12 h on a dilute NH_3 stream at 450°C [20,23]. Alongside the observations reported here, this provides a strong argument for the reusability of these composite systems.

Conclusions

Ammonia decomposition experiments, using combined mass spectrometry and flow analysis, and thermogravimetric studies were conducted on lithium amide–transition metal composite catalysts to examine their catalytic mechanism and further inform their future design for hydrogen production from ammonia. $LiNH_2$–Cr and $LiNH_2$–Mn were shown to exhibit some of the best performances yet seen for these systems. Results confirmed that the formation of a cubic, non-stoichiometric phase, $Li_{1+x}NH_{2-x}$, was correlated with high catalytic activity. The formation of this phase occurred at a lower temperature in $LiNH_2$–Cr and $LiNH_2$–Mn systems and correspondingly the catalytic activity was enhanced. These results suggest Cr and Mn promote catalysis by destabilising $LiNH_2$, such that the catalytically active solid solution phase forms at lower temperatures. Post-catalytic evidence of lithium ternary nitrides was found for both enhanced systems and these may play a part in catalysis alongside the solid solution phase, for example in a multi-site catalytic mechanism similar to those reported previously for M-N(-H)–M systems. Overall, the precise nature of the catalytic mechanism and relative importance of each reaction process remains a subject of ongoing investigation, and future *in situ* neutron diffraction studies of these systems will focus on revealing the active catalyst composition and the presence of ternary nitrides at high ammonia conversions.

Funding Information

This work was financially supported by an EU Horizon 2020 Grant: “Advanced Materials and Reactors for Energy Storage through Ammonia” (TJW) and a UKRI Future Leaders Fellowship (MR/S03403X/1) (JWM and CABD).

Conflicts of Interest

TJW is a co-founder of Sunborne Systems Ltd. The funders had no role in the design of the study; in the collection, analyses, or interpretation of data; in the writing of the manuscript, or in the decision to publish the results. All other authors had no competing interests.

Acknowledgments

Acknowledgement is given to the Diamond Light Source for the allocation of experimental time. Dr. Matthew Cummings, Dr. Jake Brittain, and Dr. James Taylor are thanked for laboratory support. Thanks is also given to Professor Bill David for helpful discussions.

References

1. The Royal Society. Ammonia: zero-carbon fertiliser, fuel and energy store. 2020.
2. IEA. Ammonia Technology Roadmap. 2021. https://www.iea.org/reports/ammonia-technology-roadmap. (Accessed 10 Jan 2022).
3. ICSC 0001 - Hydrogen. 2014. http://www.ilo.org/dyn/icsc/showcard.display?p_card_id=1&p_edit=&p_version=2&p_lang=en. (Accessed 10 Jan 2022).
4. Appl M. Ammonia. In: Ullmann's Encyclopedia of Industrial Chemistry. Weinheim, Germany: Wiley-VCH Verlag GmbH & Co. KGaA, 2006. pp. 1–155. DOI: https://doi.org/10.1002/14356007.a02_143.pub2.
5. Jan Duijm N, Markert F, Lundtang Paulsen J. Safety assessment of ammonia as a transport fuel. 2005.
6. Makepeace JW, He T, Weidenthaler C, Jensen TR, Chang F, Vegge T, et al. Reversible ammonia-based and liquid organic hydrogen carriers for high-density hydrogen storage: Recent progress. *Int J Hydrogen Energy*. 2019, 44(15): 7746–67. DOI: https://doi.org/10.1016/j.ijhydene.2019.01.144.
7. Starkman ES, Newhall HK, Sutton R, Maguire T, Farbar L. Ammonia as a spark ignition engine fuel: Theory and application. 1966. DOI: https://doi.org/10.4271/660155.
8. Halseid R, Vie PJS, Tunold R. Effect of ammonia on the performance of polymer electrolyte membrane fuel cells. *J Power Sources*. 2006, 154(2): 343–50. DOI: https://doi.org/10.1016/j.jpowsour.2005.10.011.
9. Afif A, Radenahmad N, Cheok Q, Shams S, Kim JH, Azad AK. Ammonia-fed fuel cells: A comprehensive review. *Renew Sustain Energy Rev*. 2016, 60: 822–35. DOI: https://doi.org/10.1016/j/rser.2016.01.120.
10. Yin SF, Xu BQ, Zhou XP, Au CT. A mini-review on ammonia decomposition catalysts for on-site generation of hydrogen for fuel cell applications. *Appl Catalysis A: Gral*. 2004, 277(1–2): 1–9. DOI: https://doi.org/10.1016/j.apcata.2004.09.020.
11. David WIF, Makepeace JW, Callear SK, Hunter HMA, Taylor JD, Wood TJ, et al. Hydrogen Production from Ammonia Using Sodium Amide. *J Am Chem Soc*. 2014, 136(38): 13082–5. DOI: https://doi.org/10.1021/ja5042836.
12. Makepeace JW, Wood TJ, Hunter HMA, Jones MO, David WIF. Ammonia decomposition catalysis using non-stoichiometric lithium imide. *Chem Sci*. 2015, 6(7): 3805–15. DOI: https://doi.org/10.1039/c5sc00205b.
13. David WIF, Jones MO, Gregory DH, Jewell CM, Johnson SR, Walton A, et al. A mechanism for non-stoichiometry in the lithium amide/lithium imide hydrogen storage reaction. *J Am Chem Soc*. 2007, 129(6): 1594–601. DOI: https://doi.org/10.1021/ja066016s.
14. Makepeace JW, Jones MO, Callear SK, Edwards PP, David WIF. In situ X-ray powder diffraction studies of hydrogen storage and release in the Li–N–H system. *Phys Chem Chem Phys*. 2014, 16(9): 4061. DOI: https://doi.org/10.1039/c4cp00087k.
15. Zhang J, Hu YH. Intermediate species and kinetics of lithium imide decomposition. *Int J Hydrogen Energy*. 2012, 37(13): 10467–72. DOI: https://doi.org/10.1016/j.ijhydene.2011.12.061.
16. Marx R. Reindarstellung und kristallstruktur von lithiumnitridhydrid, Li4NH, Li4ND. *Zeitschrift fur Anorg und Allg Chemie*. 1997, 623(12): 1912–6. DOI: https://doi.org/10.1002/zaac.19976231215.
17. Makepeace JW, Brittain JM, Sukhwani Manghnani A, Murray CA, Wood TJ, David WIF. Compositional flexibility in Li-N-H materials: implications for ammonia catalysis and hydrogen storage. *Phys Chem Chem Phys*. 2021, 23(28): 15091–100. DOI: https://doi.org/10.1039/d1cp02440j.
18. Wood TJ, Makepeace JW, David WIF. Isotopic studies of the ammonia decomposition reaction using lithium imide catalyst. *Phys Chem Chem Phys*. 2017, 19(6): 4719–24. DOI: https://doi.org/10.1039/C6CP07734J.
19. Guo J, Wang P, Wu G, Wu A, Hu D, Xiong Z, et al. Lithium Imide Synergy with 3d Transition-Metal Nitrides Leading to Unprecedented Catalytic Activities for Ammonia Decomposition. *Angew Chemie* Int Ed. 2015, 54(10): 2950–4. DOI: https://doi.org/10.1002/anie.201410773.
20. Guo J, Chang F, Wang P, Hu D, Yu P, Wu G, et al. Highly Active MnN–Li 2 NH Composite Catalyst for Producing CO x -Free Hydrogen. *ACS Catal*. 2015, 5(5): 2708–13. DOI: https://doi.org/10.1021/acscatal.5b00278.
21. Chang F, Guo J, Wu G, Wang P, Yu P, Chen P. Influence of alkali metal amides on the catalytic activity of manganese nitride for ammonia decomposition. *Catal Today*. 2017, 286: 141–6. DOI: https://doi.org/10.1016/j.cattod.2016.09.010.
22. Makepeace JW, Wood TJ, Marks PL, Smith RI, Murray CA, David WIF. Bulk phase behavior of lithium imide-metal nitride ammonia decomposition catalysts. *Phys Chem Chem Phys*. 2018, 20(35): 22689–97. DOI: https://doi.org/10.1039/C8CP02824A.
23. Guo J, Chen Z, Wu A, Chang F, Wang P, Hu D, et al. Electronic promoter or reacting species? The

role of LiNH2 on Ru in catalyzing NH3 decomposition. *Chem Commun.* 2015, 51(82): 15161–4. DOI: https://doi.org/10.1039/C5CC04645A.

24. Ogasawara K, Nakao T, Kishida K, Ye TN, Lu Y, Abe H, et al. Ammonia Decomposition over CaNH-Supported Ni Catalysts via an NH2--Vacancy-Mediated Mars-van Krevelen Mechanism. *ACS Catal.* 2021, 11(17): 11005–15. DOI: https://doi.org/10.1021/acscatal.1c01934.

25. Ye TN, Park SW, Lu Y, Li J, Sasase M, Kitano M, et al. Vacancy-enabled N2 activation for ammonia synthesis on an Ni-loaded catalyst. *Nature.* 2020, 583(7816): 391–5. DOI: https://doi.org/10.1038/s41586-020-2464-9.

26. Ganley JC, Thomas FS, Seebauer EG, Masel RI. A priori catalytic activity correlations: The difficult case of hydrogen production from ammonia. *Catal Letters.* 2004, 96(3–4): 117–22. DOI: https://doi.org/10.1023/B:CATL.0000030108.50691.d4.

27. Abild-Pedersen F, Greeley J, Studt F, Rossmeisl J, Munter TR, Moses PG, et al. Scaling Properties of Adsorption Energies for Hydrogen-Containing Molecules on Transition-Metal Surfaces. *Phys Rev Lett.* 2007, 99(1): 016105(1-4). DOI: https://doi.org/10.1103/PhysRevLett.99.016105.

28. Boisen A, Dahl S, Nørskov JK, Christensen CH. Why the optimal ammonia synthesis catalyst is not the optimal ammonia decomposition catalyst. *J Catal.* 2005, 230(2): 309–12. DOI: https://doi.org/10.1016/j.jcat.2004.12.013.

29. Logadottir A, Rod TH, Nørskov JK, Hammer B, Dahl S, Jacobsen CJH. The Brønsted-Evans-Polanyi relation and the volcano plot for ammonia synthesis over transition metal catalysts. *J Catal.* 2001, 197(2): 229–31. DOI: https://doi.org/10.1006/jcat.2000.3087.

30. Makepeace JW, Hunter HMA, Wood TJ, Smith RI, Murray CA, David WIF. Ammonia decomposition catalysis using lithium-calcium imide. *Faraday Discuss.* 2016, 188: 525–44. DOI: https://doi.org/10.1039/c5fd00179j.

31. Wood TJ, Makepeace JW, David WIF. Neutron diffraction and gravimetric study of the iron nitriding reaction under ammonia decomposition conditions. *Phys Chem Chem Phys.* 2017, 19(40): 27859–65. DOI: https://doi.org/10.1039/c7cp04494a.

32. Arabczyk W, Zamłynny J. Study of the ammonia decomposition over iron catalysts. Catal Letters. 1999, 60(3): 167–71. DOI: https://doi.org/10.1023/A:1019007024041.

33. PubChem. Lithium amide compound summary. https://pubchem.ncbi.nlm.nih.gov/compound/Lithium-amide#section=Melting-Point. (Accessed 29 Mar 2021).

34. Davies RA, Hewett DR, Anderson PA. Enhancing ionic conductivity in lithium amide for improved energy storage materials. *Adv Nat Sci Nanosci Nanotechnol.* 2015, 6(1): 15005. DOI: https://doi.org/10.1088/2043-6262/6/1/015005.

35. Wood TJ, Makepeace JW, Hunter HMA, Jones MO, David WIF. Isotopic studies of the ammonia decomposition reaction mediated by sodium amide. *Phys Chem Chem Phys.* 2015, 17(35): 22999–3006. DOI: https://doi.org/10.1039/c5cp03560k.

36. Yang M, Raucci U, Parrinello M. Ammonia Decomposition on Lithium Imide Surfaces: A New Paradigm in Heterogeneous Catalysis. *ChemRxiv.* 2022, : preprint. DOI: https://doi.org/10.26434/chemrxiv-2022-qr7wt.

37. Markmaitree T, Ren R, Shaw LL. Enhancement of Lithium Amide to Lithium Imide Transition via Mechanical Activation. *J Phys Chem B.* 2006, 110(41): 20710–8. DOI: https://doi.org/10.1021/JP060181C.

38. Zhang T, Isobe S, Wang Y, Hashimoto N, Ohnuki S. Lithium metatitanate enhanced solid-solid reaction in a lithium-nitrogen-hydrogen system. *RSC Adv.* 2015, 5(24): 18375–8. DOI: https://doi.org/10.1039/c5ra00285k.

39. Palade P, Lungu GAA, Husanu AMM. Thermodynamic destabilization of Li–N–H system by Si addition. *J Alloys Compd.* 2010, 505(1): 343–7. DOI: https://doi.org/10.1016/j.jallcom.2010.03.249.

40. Zhang J, Hu YH. Decomposition of lithium amide and lithium imide with and without anion promoter. *Ind Eng Chem Res.* 2011, 50(13): 8058–64. DOI: https://doi.org/10.1021/ie2008696.

41. Bahou S, Labrim H, Ez-Zahraouy H. Improvement of decomposition temperature and gravimetric density of MgH2 by transition metals and vacancies: A comparison study. *Solid State Commun.* 2023, : 115170. DOI: https://doi.org/10.1016/j.ssc.2023.115170.

42. Tapia-Ruiz N, Segalés M, Gregory DH. The chemistry of ternary and higher lithium nitrides. *Coord Chem Rev.* 2013, 257(13–14): 1978–2014. DOI: https://doi.org/10.1016/j.ccr.2012.11.008.

43. Brittain JM. Structural and Spectroscopic Investigations into the Non-Stoichiometric Phases in the Lithium Amide-Imide System. Master's thesis. University of Oxford, 2017.

44. Searle JR. Synthesis and characterisation of the catalytically active Li-Mn-N system. Master's thesis. University of Oxford, 2018.

45. Bindi L, Cámara F, Gain SEM, Griffin WL, Huang J-X, Saunders M, et al. Kishonite, VH2, and Oreillyite, Cr2N, Two New Minerals from the Corundum Xenocrysts of Mt Carmel, Northern Israel. Minerals. 2020, 10(12): 1118. DOI: https://doi.org/10.3390/min10121118.

46. Leineweber A, Jacobs H, Kockelmann W. Nitrogen ordering in ζ-manganese nitrides with hcp

arrangement of Mn - MnNy with 0.39 < y < 0.48 - Determined by neutron diffraction. *J Alloys Compd.* 2004, 368(1–2): 229–47. DOI: https://doi.org/10.1016/j.jallcom.2003.08.062.